Diffusion Monte Carlo study of jellium surfaces: Electronic densities and pair correlation functions

Paulo H. Acioli
Departamento de Física, Universidade de Brasília, Brasília, Distrito Federal, 70.910-900, Brazil

D. M. Ceperley
National Center for Supercomputing Applications, Physics Department, University of Illinois at Urbana-Champaign, Urbana, Illinois 61801

(Received 23 April 1996; revised manuscript received 29 July 1996)

We present the results of fixed-node diffusion Monte Carlo calculations of jellium surfaces for metallic densities. We used a trial wave function of the Slater-Jastrow type, with the long-range part of the two-body term modified to account for the anisotropy of the system. The one-body term is optimized so that the electronic density from variational and diffusion Monte Carlo calculations agree with each other. The final densities are close to the densities obtained from density-functional calculations in the local-density approximation and the surface energies to the results obtained using the Langreth-Mehl and Perdew-Wang generalized gradient approximation at high densities ($r_s \leqslant 2.07$). At low densities ($r_s \geqslant 3.25$) they agree with the results of the Fermi-hypernetted-chain calculations. The pair-correlation functions at regions near the surface are tabulated, showing the anisotropy of the exchange-correlation hole in regions of fast-varying densities. [S0163-1829(96)06848-8]

I. INTRODUCTION

The jellium surface is the simplest model for simple metal surfaces and a prototype to study correlation effects in inhomogeneous systems. In systems with only a few electrons correlation can be determined using quantum chemistry methods; however, for extended systems such methods are not feasible. Hohenberg and Kohn[1] have shown that the effects of exchange and correlation can be formally expressed in terms of an universal functional of the density, $E_{\rm xc}[n]$. Although the theory is formally exact, in practice approximations to the exchange-correlation functional are needed. Among them, the simplest, and the most used, is the local-density approximation (LDA),[2] which assumes a slowly varying density. Although LDA has enjoyed great success in qualitatively and semiquantitatively explaining electron correlation effects, its application to highly inhomogeneous systems is questionable. Corrections to the LDA, all assume, in some degree, slowly varying densities. Because of their simplicity, jellium surfaces play an important role in the development of such approximations. It has been used both as a case study and as a testing ground for the development of new approximations. For this reason it would be very useful to determine correlation effects in such systems exactly. In this work we study jellium surfaces using fixed-node diffusion Monte Carlo[3] (DMC), which has been demonstrated to determine accurately correlation effects in both homogeneous and inhomogeneous systems.

This work is the extension of the work of X.-P. Li *et al.*[4] for a jellium slab (electron gas) at the average valence density of aluminum ($r_s = 2.07$). The surface energy computed in their work was in agreement with results from a density-functional theory (DFT) calculation[5] using the Langreth-Mehl[6] nonlocal exchange-correlation functional. We study jellium slabs at five different densities ($r_s = 1.87,\ 2.07,\ 2.66,\ 3.25,\ 3.93$) using better-optimized wave functions and conclude that the surface energies agree with the DFT results using the Langreth-Mehl[5] (LM) and the Perdew-Wang[7] functionals only at the high-density regime ($r_s = 1.87,\ 2.07$). In the low-density regime ($r_s = 2.66,\ 3.25,\ 3.93$) our results approach those from the Fermi-hypernetted-chain (FHNC) calculations of Krotscheck *et al.*[8] The density profiles obtained using DMC differ from the LDA calculations (in the same geometry) by about 2% (roughly the uncertainty of the DMC), confirming the initial assumption that the LDA densities are quite accurate. The work functions computed using DMC lie, on average, about 0.5 eV lower than those from LDA,[5] in qualitative agreement with the FHNC results, which lie about 0.3 eV lower than the LDA results.

One of the key quantities computed in this work is the pair correlation function, as there is an exact expression of the exchange-correlation functional in terms of this function.[9–11] We computed and tabulated the pair correlation functions at regions near the edge of the slab. Inside the slab, the exchange-correlation hole is nearly spherical but as the electron is moved towards the edge of the slab, the hole flattens out, elongated in the direction normal to the surface.

This paper is organized as follows. In the next section we will discuss the jellium model and present a brief summary of the main results in the literature. In Sec. III A we present some basic aspects of diffusion Monte Carlo and the details of the calculations in this work. In Sec. IV we discuss the density profiles, work functions, surface energies, and pair correlation functions. The conclusion follows. We tabulate the pair correlation functions at various densities and they are available from the Electronic Physics Auxiliary Publication Service (E-PAPS).[12]

II. THE JELLIUM MODEL

The jellium model of a metal consists of electrons moving a uniform positive background of equal charge. The properties of the system are determined by its electronic density (n_0) or equivalently by its Wigner-Seitz radius $r_s=(4\pi/3n_0)^{1/3}$. This model describes the simple (s-p bonded) metals and is the starting point of the approximations of DFT, such as the LDA. A jellium surface can be formed by terminating the positive background at a plane. This positive background density will create an external potential $v(z)$ in which the electrons move. The Hamiltonian of the system (in atomic units) is then

$$H=-\sum_i \frac{1}{2}\nabla_i^2-\sum_{i<j}\frac{1}{r_{ij}}+\sum_i v(z_i)+\text{ const.} \tag{1}$$

Lang and Kohn[13,14] performed the first self-consistent calculation of jellium surfaces within the framework of DFT in the LDA. Their work gives a qualitative and quantitative description of jellium surfaces which are summarized in the next paragraphs.

Typical electron densities from a LDA calculation fall off exponentially outside the surface and exhibit Friedel-like oscillations in the bulk, with a characteristic wavelength of half the Fermi wavelength.[13] The amplitude of these oscillations decays with the square of the distance from the surface plane ($z=0$). The spilling out of electrons from the positive background creates a dipole barrier at the surface, an important contribution to the work function. Lang and Kohn[14] showed, in fact, that the work function can be rigorously written as

$$W=\overline{D}-\overline{\mu}, \tag{2}$$

where $\overline{D}=\phi(\infty)-\overline{\phi}$ and $\overline{\mu}=\mu-\overline{\phi}$ are the dipole barrier and bulk chemical potential measured from the average electrostatic potential inside the crystal $\overline{\phi}$. The calculations of the work functions by Lang and Kohn[13,14] in the jellium model showed a qualitative agreement with experiment, and were further improved by including effects of the ionic lattice using perturbation methods.[13,14]

Another important quantity is the surface energy, which is defined as the work required to split the crystal along a given plane, i.e.,

$$\sigma=\frac{(E_s-E_c)}{2A}, \tag{3}$$

where E_c is the energy of the crystal (in this case the electron gas) before it is split, E_s is the energy after it is split, and A is the area of each surface formed. The LDA calculations of Lang and Kohn showed that the surface energies in the jellium models are negative at high densities ($r_s<2.4$). The origin of negative surface energies lies in the fact that the electron gas is not at mechanical equilibrium at all densities. A stabilized jellium model has been proposed that corrects this problem.[15]

III. QMC SIMULATIONS OF JELLIUM SLABS

A. Computational details

We use a rectangular supercell (dimensions L_x, L_y, and L_z) with periodic boundary conditions in all three directions. Our model system is a finite slab of jellium separated by a vacuum region. This kind of slab geometry has been widely used in surface electronic structure calculations.[8,16] It produces reliable results, provided the slab is sufficiently thick. The positive background density is given by

$$n_+(z)=\begin{cases} n_0, & |z|\leqslant s \\ 0, & s<|z|<L_z/2, \end{cases} \tag{4}$$

where $-s$ and s are the positions of the edges of the slab and L_z is the length of the box in the z direction. The uniform part of the electronic density plus the background density gives rise to the parabolic potential

$$v(z)=\begin{cases} 2\pi n_0[-s(L_z-s)(L_z-2s)/3L_z+(L_z-2s)z^2/L_z], & |z|\leqslant s \\ 2\pi n_0[-s(L_z-s)(L_z-2s)/3L_z+s(-2z^2+2|z|L_z-sL_z)/L_z], & s<|z|<L_z/2. \end{cases} \tag{5}$$

The electrostatic energy contribution due to the positive background and the uniform component of the electronic density is

$$E_{\rm el}=L_xL_yL_z\frac{2\pi n_0^2 s^2}{3L_z^2}(L_z-2s)^2. \tag{6}$$

For our calculation we used an orthorhombic supercell, square in the xy plane, with dimensions $L_x=L_y=5.57r_s$ Å, $L_z=7.63r_s$ Å, and $s=L_z/4$, with periodic boundary conditions in all three directions. The thickness of the slab was chosen to hold five layers of (bcc) sodium with surface normal to the [110] direction. For the sake of comparison we kept the same aspect ratio for the simulations at all densities. The vacuum region was chosen to have the same thickness as the jellium slab to minimize interaction between electrons in the vacuum regions from opposite sides of the slab.

Two ground-state quantum Monte Carlo methods, variational Monte Carlo (VMC) and DMC, are used in this work. Variational methods[17] that use explicitly correlated wave functions are particularly appealing since one can determine in a more transparent way the nature of correlation effects. However, such methods should be used with caution to compute energy differences, like surface and cohesive energies, since there can be a bias towards one of the systems, bulk or surface. A more attractive approach is DMC, since the projection operator will eliminate most of this bias.

The trial wave function we used is of the pair-product form (Slater-Jastrow) with a one-body correlation term $\chi(\mathbf{r})$,

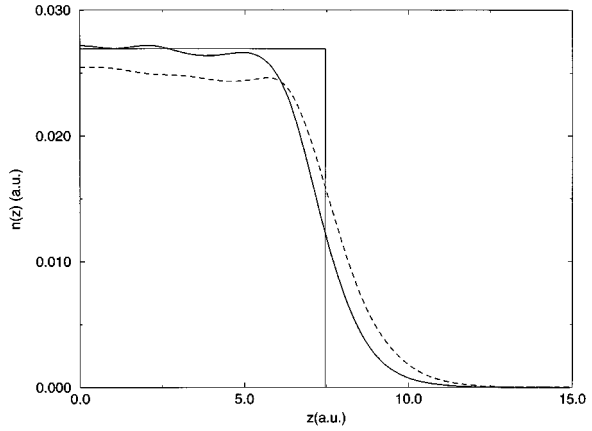

FIG. 1. Effects of the two-body term in the wave function on the density of jellium surfaces. The solid line is the density from the single-particle wave function. The dashed line is the density of the single-particle plus two-body term wave function. VMC calculations of $r_s = 2.07$.

$$\Psi(\mathbf{R}) = D(\uparrow)D(\downarrow)\exp\left[\sum_i \chi(\mathbf{r}) + \sum_{i<j} u(\mathbf{r}_{ij})\right]. \quad (7)$$

The single-particle orbitals in the Slater determinants $D(\uparrow)D(\downarrow)$ are obtained from a LDA calculation using the Perdew-Zunger[18] parameterization of the electron gas correlation energies of Ceperley and Alder.[19] The two-body correlation function $u(\mathbf{r}_{ij})$ used in QMC simulation of the three-dimensional electron gas is obtained from the RPA, and its form in Fourier space[17] is

$$u(\mathbf{k}) = -\frac{1}{2S_0(\mathbf{k})} + \left[\frac{1}{4S_0(\mathbf{k})^2} + \frac{V(k)}{k^2}\right]^{1/2}, \quad (8)$$

where $S_0(\mathbf{k})$ is the static structure factor of the homogeneous electron gas and $V(k)$ is the Fourier transform of the interparticle potential $[V(k) = 4\pi e^2/k^2]$.

This function is long-ranged in real space, so it is usually broken into a short-range part (u_s) in real space and a long-range (u_l) part, which is represented in Fourier space:

$$u(\mathbf{r}_{ij}) = u_s(\mathbf{r}_{ij}) + \sum_{\mathbf{k}} u_l(\mathbf{k})\exp(i\mathbf{k}\cdot\mathbf{r}_{ij}). \quad (9)$$

This two-body wave function gives very good results when applied to nearly homogeneous systems, but its application to jellium surfaces is poor. The VMC energies are higher than the energies using only the single-particle part of the wave function. X.-P. Li and co-workers[4] have found it necessary to modify the long-range part of Eq. (9), by eliminating terms with $k_z \neq 0$. The use of this modified version of the two-body wave function recovers about 90% of the difference between the single particle and exact (DMC) energies. The cusp conditions are enforced in the short-range part of the two-body term.

The role of the one-body term is to make corrections to the density. Fahy and Louie[20] observed that the two-body wave function, the primary role of which is to create a correlation hole, changes the density of the system with a tendency towards a more homogeneous system (Fig. 1). They proposed a one-body wave function of the form

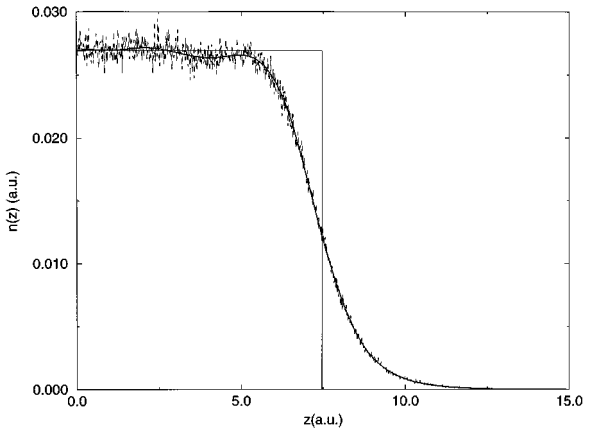

FIG. 2. VMC density before smoothing (dashed line). VMC density after cubic spline smoothing (solid line). Density at $r_s = 2.07$.

$$\chi(\mathbf{r}) = 0.5\alpha\ln\left(\frac{n_{\rm sp}(\mathbf{r})}{n_{\rm VMC}(\mathbf{r})}\right), \quad (10)$$

where α is an adjustable parameter and $n_{\rm sp}$ and $n_{\rm VMC}$ are the densities obtained from the single-particle and VMC calculations, respectively. This term is adjusted until the VMC and single-particle densities agree with each other. Details of the optimization will be given below.

After the optimization of the trial wave function is complete we are ready to perform a DMC simulation of the system (for details see Ref. 3). In DMC the energies are computed exactly but for other operators that do not commute with the Hamiltonian we define a mixed estimate,[21]

$$\langle\hat{O}\rangle_{\rm mix} = \frac{\int d\mathbf{R}\Phi_0(\mathbf{R})\hat{H}\Psi(\mathbf{R})}{\int d\mathbf{R}\Psi(\mathbf{R})\Phi_0(\mathbf{R})}. \quad (11)$$

The error associated with this estimate is linear in the difference between the ground state and the trial wave functions. A better estimator is a simple linear extrapolation, which preserves sum rules,

$$\langle\hat{O}\rangle_{\rm ext} = 2\langle\hat{O}\rangle_{\rm mix} - \langle\hat{O}\rangle_{\rm var}, \quad (12)$$

where $\langle\hat{O}\rangle_{\rm var}$ is the variational estimator. One can easily show that the error from this estimator is quadratic in the difference between the trial and ground-state wave functions. For positive definite quantities like densities and pair correlation functions, it is better to use a geometric extrapolation,[22]

$$\langle\hat{O}\rangle_{\rm ext} = \frac{\langle\hat{O}\rangle^2_{\rm mix}}{\langle\hat{O}\rangle_{\rm var}}, \quad (13)$$

because this preserves positivity. In the limit of very accurate wave functions both estimators yield the same answer and both are correct to order $(\Psi - \Psi_0)$.

We use the fixed-node approximation[3] to enforce antisymmetry in the wave function. The energy so obtained will be an upper bound on the ground-state energy. There exist exact fermion procedures known as the release-node[23] or the transient-estimate[18] methods, but these methods are too slow

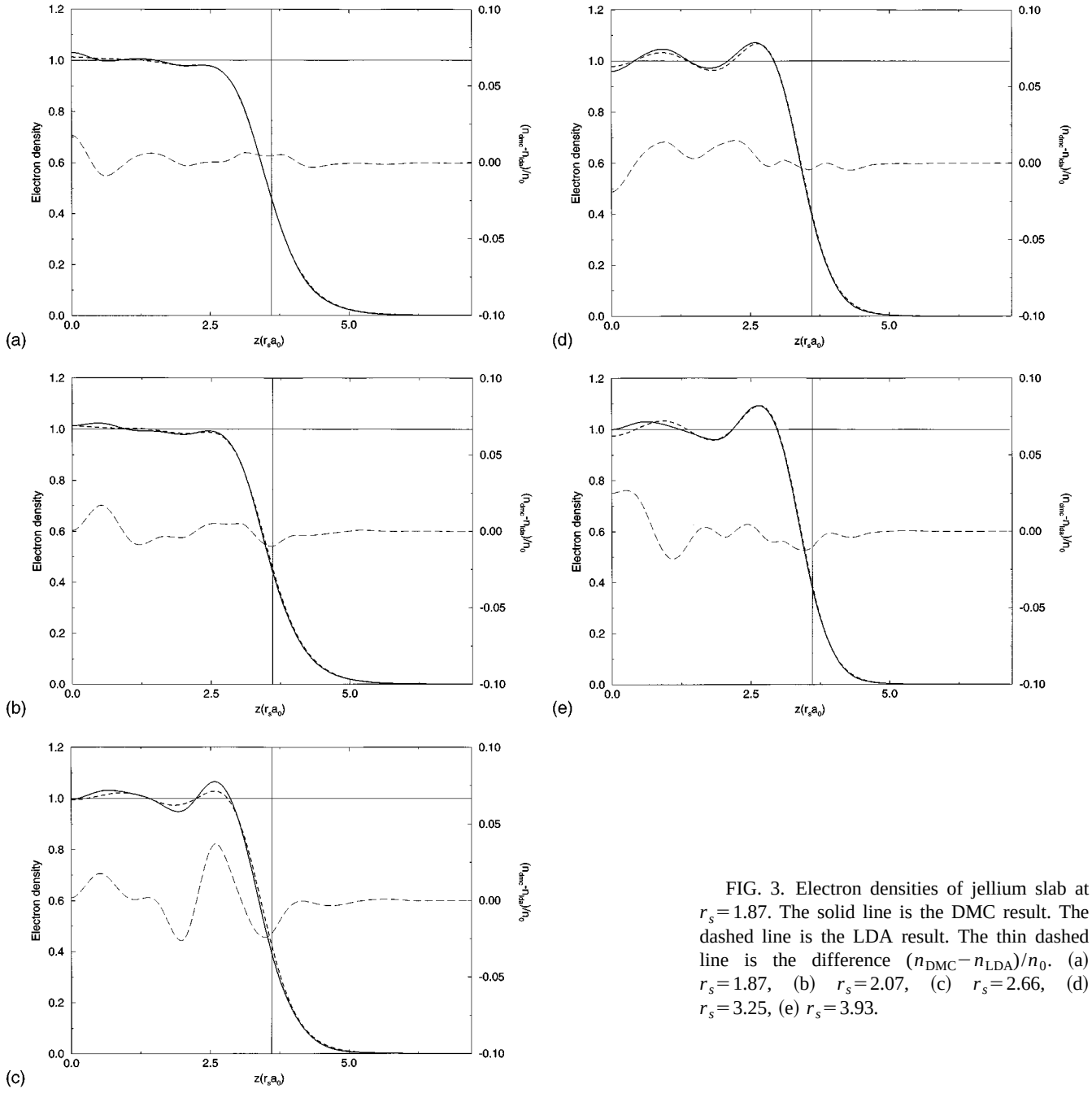

FIG. 3. Electron densities of jellium slab at $r_s=1.87$. The solid line is the DMC result. The dashed line is the LDA result. The thin dashed line is the difference $(n_{\mathrm{DMC}}-n_{\mathrm{LDA}})/n_0$. (a) $r_s=1.87$, (b) $r_s=2.07$, (c) $r_s=2.66$, (d) $r_s=3.25$, (e) $r_s=3.93$.

for the many-electron system considered here. The fixed-node approximation has been shown to give excellent results for the electron gas.[18,24]

IV. RESULTS

A. Density profiles

Accurate determination of the work function and the pair correlation functions depend on the accuracy of the density profile. The electronic densities determine the dipole barrier at the surface and consequently the work function of the system. The output of a QMC simulation is the average density $\overline{n(z_i)}$ at a point z_i with an error $\Delta\overline{n(z_i)}$. Figure 2 shows a typical density output from a VMC simulation at $r_s=2.07$ with statistical error. To smooth the density out we use a smooth function $n_s(z_i,\{\lambda_j\})$ of parameters $\{\lambda_j\}$, and minimize

$$\chi^2(\{\lambda_j\})=\sum_{i=1}^{N_{\mathrm{dat}}}\left(\frac{n_s(z_i,\{\lambda_j\})-\overline{n(z_i)}}{\Delta n(z_i)}\right) \tag{14}$$

with respect to $\{\lambda_j\}$. We choose a cubic spline interpolation as our smoothing function,[25] the variational parameters are the values of the function at the chosen spline knots (z_i's). A set of 15 knots was sufficient to smooth out the original data set of 1000 grid points. This procedure yields very smooth densities (see Fig. 1) without the oscillations coming from the Fourier smoothing method used in Ref. 4.

TABLE I. LDA work functions for a finite jellium slab. W(LDA) is the LDA work function for the finite slab using the supercell geometry. W(VWN) are the LDA work functions for the semi-infinite model of a jellium surface extrapolated from Ref. 5.

r_s	$\overline{\mu}=\frac{1}{2}k_F^2+\mu_{xc}$	$\overline{D}$	W (LDA)	W (VWN)
1.87	3.99	8.92	4.93	3.84
2.07	2.28	5.15	2.87	3.79
2.66	-0.42	3.55	3.97	3.55
3.25	-1.51	2.05	3.56	3.26
3.93	-2.02	0.54	2.56	2.96

It is obvious from Fig. 1 that a good optimization of the one-body term in the trial wave function is necessary to obtain a reasonable VMC density. Since the density from the LDA calculation is expected to be a reasonable approximation to the ground-state density, the first step in the optimization was to make the VMC and LDA densities as close as possible. This was done by running a VMC simulation without the one-body term and using that to estimate the correction through Eq. (10). The procedure is then repeated with the one-body term present in the trial wave function until both the VMC and LDA densities agree. After a good guess for the density is obtained, we perform a DMC simulation and estimate the ground-state density. Finally, we adjust the one-body term so that VMC and the density using the mixed estimator Eq. (11) agree with each other. This corresponds to maximizing the overlap between Ψ and Φ.[26] We then use the extrapolated estimator Eq. (12) to obtain the final DMC densities. The densities obtained with this procedure are shown in Figs. 3. Also shown are the LDA densities (obtained in a calculation with the same supercell) and the difference between the DMC and LDA densities divided by n_0.

The densities we obtained from DMC are in close agreement with LDA densities, with differences of the order of 2%, with the exception of $r_s=2.66$, where the differences are more pronounced. At $r_s=2.66$ there is a tendency to increase the strength of the Friedel-like oscillations, a behavior not observed at the other densities. Because there is no particular pattern in the difference between the DMC and LDA densities, we cannot conclude that the differences are significant.

B. Work functions

To compute the work function we use Eq. (2), derived for a semi-infinite model of a jellium surface. The problem in using such an expression is that in a slab of finite thickness the Friedel oscillations have not completely died out at the center of the slab, introducing an uncertainty in the computation of the electrostatic barrier. To correct for such an effect we computed the electrostatic barrier in the same supercell geometry using the LDA density profiles and compared with the LDA results of Zhang *et al.* for the semi-infinite jellium surface, using the Vosko-Wilk-Nussair[27] formula for exchange and correlation. The difference between them is an estimate of the correction due to the finite thickness of the slab.

TABLE II. Contributions to the QMC work-function jellium surface. $\overline{D}$ is the electrostatic barrier. ΔW_{LDA} is a correction due to the finite thickness of the slab. $W=\overline{D}-\overline{\mu}+\Delta W_{\mathrm{LDA}}$.

r_s	$\overline{D}$	ΔW_{LDA}	W(QMC)
1.87	8.67	-1.09	3.59 (28)
2.07	4.44	0.92	3.08 (28)
2.66	2.68	-0.42	2.68 (28)
3.25	1.90	-0.30	3.11 (28)
3.93	-0.18	0.40	2.24 (28)

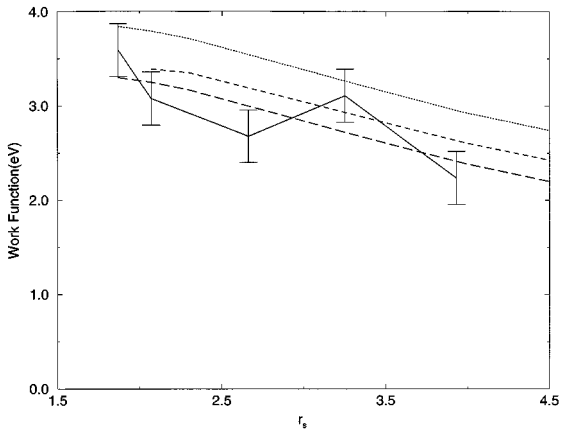

FIG. 4. Work functions computed with QMC (solid line with error bars), LDA (dotted line), FHNC (dashed line) and LDA work function minus the average drop of the QMC electrostatic barrier with respect to LDA (long-dashed line).

Table I displays the work functions of a jellium slab computed in a LDA calculation using the same supercell used in the QMC calculations. Shown in the table are the chemical potential, the electrostatic barrier, the work function of the finite slab and the work function of the semi-infinite jellium.[5] In Table II we present the electrostatic barrier, the finite thickness correction $\Delta W_{\mathrm{LDA}}=W$ (VWN) $-W$ (LDA), and the estimate of the work function computed using QMC. The main difference between the LDA and QMC results for the work function of the finite slab is the electrostatic barrier. Tables I and II show that the electrostatic barriers in QMC are smaller than those in LDA. The drop in the electrostatic barrier does not follow any specific trend, ranging from -0.15 to -0.86 eV, again suggesting that there is statistical and systematic uncertainty in the determination of the QMC density profiles. The change averaged over all densities is -0.54 eV, with a standard deviation of 0.28 eV. In Fig. 4 we compare Zhang *et al.* work functions with the QMC work function of Table II, the LDA work functions minus the average drop in the electrostatic barrier and the FHNC work functions for a finite slab as computed by Zhang *et al.*. A more accurate determination of the work function using QMC requires much longer runs in order to eliminate the statistical fluctuation in electron density profiles and a simulation of slabs that are thick enough to avoid the rather uncertain finite thickness correction.

Although the uncertainty in our calculation of the work function is rather high, due to the uncertainty in the density profiles and the finite thickness correction, our results indicate that the work functions computed using QMC lie about

TABLE III. Energies in eV of a jellium slab as a function of r_s. SP-VMC is the VMC energy from the single-particle part of the trial wave function. VMC is the energy using the optimized trial function. DMC are the fixed-node energies. LDA_1 is the LDA energy of the supercell calculation. LDA (full) are the energies from the fully converged LDA calculation of the slab geometry. The numbers in parentheses are the error bars in the last digit.

r_s	LDA_1	LDA (full)	SP-VMC	VMC	DMC
1.87	0.6056	0.5549	1.72 (1)	0.721 (4)	0.6444 (8)
2.07	-0.2242	-0.2654	0.842 (8)	-0.125 (5)	-0.2090 (5)
2.66	-1.4584	-1.4857	-0.48 (1)	-1.334 (3)	-1.4376 (8)
3.25	-1.8957	-1.9134	-0.99 (1)	-1.787 (3)	-1.8659 (5)
3.93	-2.0403	-2.0481	-1.212 (5)	-1.919 (2)	-2.0092 (4)

0.5 eV lower than the LDA work functions. These results are in agreement with the FHNC calculation of the work functions as computed by Zhang *et al.*, which lie about 0.3 eV lower than LDA. The work functions from a DFT calculation using the Perdew and Wang[28] GGA are lower than LDA, although for the cases studied the drop was not constant. In contrast, the work functions computed using the Langreth-Mehl[5] GGA are higher by about 0.3 eV.

C. Surface energies

One of the surface properties most sensitive to correlation effects is the surface energy. The surface energy is computed from Eq. (3). The energy of the homogeneous electron gas is obtained from the Perdew-Zunger[18] parametrization of the Ceperley-Alder[19] correlation energies. We studied equivalent LDA calculations performed in a unit cell with same L_z as the supercell, but L_z and L_y are adjusted so the unit cell contains only one electron. To obtain the single-particle orbitals and the energy corresponding to the supercell, the integrals in k_x-k_y space are performed using k points corresponding to the Γ point of the supercell. To obtain the full LDA energy of the slab we used a large set of Monkhorst-Pack[29] special points in the xy plane. We then made a finite size correction to the QMC data equal to the difference between the full LDA energy and the energy of the LDA calculation in the supercell.

Table III displays the energies in eV/electron of the jellium slabs as a function of r_s. In order to show how important correlation is and the accuracy of the pair-product wave function, we show the trial energy for the single-particle (SP-VMC) part of the wave function (Slater determinant of the LDA orbitals), the VMC energy with the optimized trial wave function, including the one- and two-body terms and the fixed-node energies. Also displayed are the LDA energies of the supercell and the energies from the full LDA calculation for the slab geometry. The VMC energies recover about 90% of the difference between the DMC and the single-particle energies, typical values for a pair-product wave function.[23]

Inspection of Table III shows that the LDA energies are lower than the DMC energies by about 0.02 eV. This small difference is very significant in the computation of the surface energies, since the QMC and LDA energies for the homogeneous electron gas are identical. This can be seen by comparing the surface energies in Table IV. The error bars displayed in Table IV are estimated as a sum of several contributions: (a) the time step error, which we believe is negligible; (b) the finite size error, which we roughly estimate as 10% of the LDA correction; (c) the fixed-node error, which we estimate as the release-node correction of the homogeneous electron gas. At $r_s=2.07$ this correction[4] is -0.0023 eV or about 0.2% of the correlation energy of the homogeneous electron gas; (d) statistical error.

The agreement between the LDA surface energies obtained from Table IV and the ones from Ref. 5 gives us confidence that although our QMC numbers were computed using a finite slab, the correction for the semi-infinite case should be small. In Fig. 5 we compare the surface energies obtained in this work with the surface energies of Zhang *et al.*, computed using the LDA (using the Vosko-Wilk-Nussair formula[27] for E_c) and the nonlocal Langreth-Mehl[6] (LM-DFT) exchange-correlation functional. Also shown are the surface energies obtained by Krotscheck *et al.* using FHNC. The calculations of Zhang *et al.* were performed in the semi-infinite jellium model and can be considered the extrapolation of our LDA energies for infinite slab thickness. The agreement between our LDA energies (open circle) and the LDA energies of Zhang *et al.* (open triangles) suggests that the correction from such extrapolation are small. A comparison of the DMC results (stars and dashed lines) with the LM-DFT (open squares) and FHNC (filled triangles) surface energies show that at high densities the QMC results agree with the LM-DFT and at low densities they approach the FHNC results. At $r_s=2.07$ our surface energy agrees, within error bars, with the calculation of X.-P. Li *et al.* of $-0.029\ (3)$ eV/Å^2.

Another important quantity is the correlation contribution to the surface energy (surface correlation energy) defined as the difference between the exact surface energy and the surface energy in the HF approximation. Upper bounds for the

TABLE IV. Surface energies in the jellium model. $E_{\rm bulk}$ is the energy of the homogeneous electron gas. LDA is the surface energy obtained from LDA. QMC is the surface energy obtained from the DMC calculation corrected for finite size effects, with error bars.

r_s	$E_{\rm bulk}$ (eV)	LDA (eV/Å^2)	QMC (eV/Å^2)
1.87	0.6671	-0.0986	-0.065 (8)
2.07	-0.2140	-0.0368	-0.026 (5)
2.66	-1.5119	0.0113	0.020 (3)
3.25	-1.9620	0.0141	0.023 (2)
3.93	-2.1062	0.0115	0.018 (1)

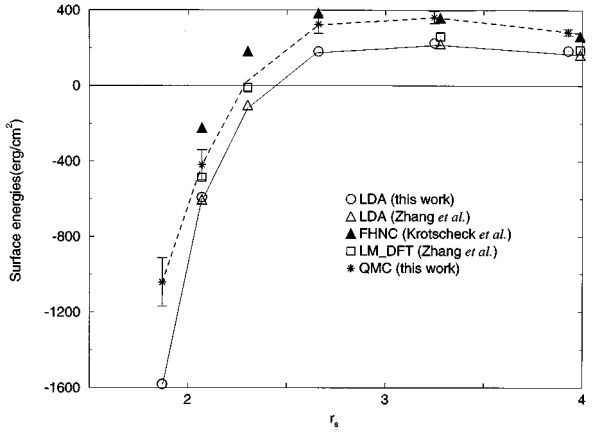

FIG. 5. Surface energies. The open circles represent the LDA calculation for this work. The open triangles are the LDA results of Zhang *et al.* The open squares are the LM-DFT results of Zhang *et al.* The filled triangles are the FHNC results of Krotscheck *et al.*

HF surface energies have been computed by Sahni and Ma[30] and by Krotscheck and Kohn[31] using the Talman-Shadwick procedure[32] for exchange-only calculations. We use the HF energies of Krotscheck and Kohn, since they are lower than the energies of Sahni and Ma. In Table V we compare the surface correlation energies computed in this work with interpolated values from Krotscheck and Kohn. As already demonstrated in Fig. 5 they agree at high values of r_s, where FHNC is expected to be accurate,[33] while at low values[34] of r_s the FHNC surface correlation energies are too low.

D. Pair correlation functions

The pair correlation function near the jellium surface provides useful information about the pair correlation in inhomogeneous systems. The exchange and correlation functional has an exact expression in terms of pair correlation functions[9–11]

$$E_{\rm xc}[n]=\int d\mathbf{r}d\mathbf{r}'\,\frac{n(\mathbf{r})n(\mathbf{r}')}{|\mathbf{r}-\mathbf{r}'|}\int_0^{e^2=1}d\lambda[g_\lambda(\mathbf{r},\mathbf{r}')-1] \tag{15}$$

where $g_\lambda(\mathbf{r},\mathbf{r}')$ is the pair correlation function corresponding to the $e-e$ strength (charge) λ.

TABLE V. Surface correlation energies in erg/cm^2. σ_{HF} are Hartree-Fock surface energies interpolated from the data computed in Ref. 31. σ_c (FHNC) are the surface correlation energies from FHNC calculations. σ_c (QMC) are the surface correlation energies from QMC.

r_s	$\sigma_{\rm HF}$	σ_c (FHNC)	σ_c (QMC)
1.87	-2068		1027
2.07	-1273	1021	856
2.66	-215	598	540
3.25	1		362
3.28	5	355	
3.93	41		242
3.99	40	221	

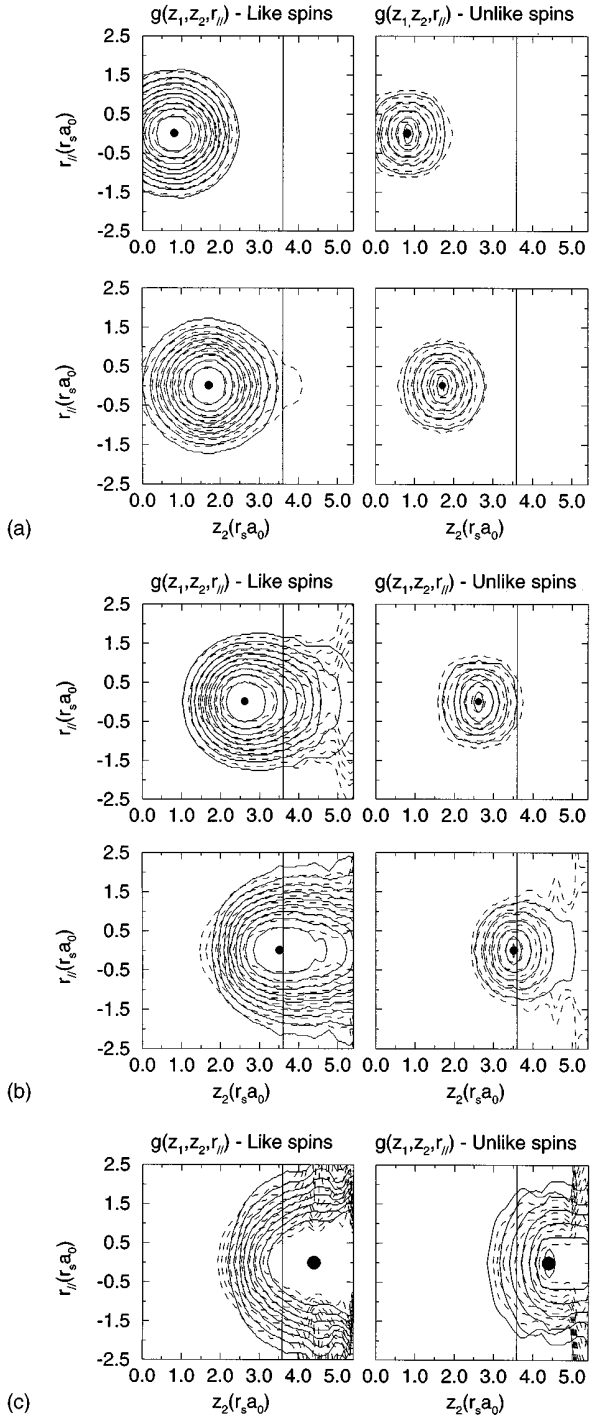

FIG. 6. (a) Contour plots of pair correlation functions for jellium surfaces. Top figures, $z_1=0.86r_sa_0$. Bottom figures, $z_1=1.72r_sa_0$. Left (like spins), right (unlike spins). The full lines are for $r_s=1.87$. The dashed lines are for $r_s=3.93$. The vertical lines represent the edge of the positive background. The circles represent z_1. (b) Contour plots of pair correlation functions for jellium surfaces. Top figures, $z_1=2.61r_sa_0$. Bottom figures, $z_1=3.51r_sa_0$. Left (like spins), right (unlike spins). The full lines are for $r_s=1.87$. The dashed lines are for $r_s=3.93$. The vertical lines represent the edge of the positive background. The circles represent z_1. (c) Contour plots of pair correlation functions for jellium surfaces. $z_1=4.40r_sa_0$. The full lines are for $r_s=1.87$. The dashed lines are for $r_s=3.93$. The vertical lines represent the edge of the positive background. The circles represent z_1.

In our model system, the inhomogeneity is along the z direction, so we computed the pair correlation function for a pair of electrons as a function of z_1 and z_2, and their azimuthal distance $r_\parallel = \sqrt{(x_1-x_2)^2+(y_1-y_2)^2}$,

$$g(z_1,z_2,r_\parallel) = \frac{\rho^{(2)}(z_1,z_2,r_\parallel)}{\rho^{(1)}(z_1)\rho^{(1)}(z_2)}. \tag{16}$$

Because local spin density methods (LSD) treat particles with like and unlike spins differently, we have computed Eq. (16) for like ($\uparrow\uparrow$ or $\downarrow\downarrow$) and unlike spins ($\uparrow\downarrow$ or $\downarrow\uparrow$), separately. The pair correlation functions are computed in a three-dimensional grid in real space. Smoothed pair correlation functions are obtained using the same cubic spline fitting used for the density profiles, with the additional constraints

$$g(z_1,z_1,0) = 0 \text{ for like spins,} \tag{17}$$

$$\frac{dg(z1,z1,0)}{dr_\parallel} = g(z_1,z_1,0), \tag{18}$$

and

$$\frac{dg(z1,z2,0)}{dr_\parallel} = 0 \text{ for } z_1 \neq z_2. \tag{19}$$

The first constraint is the Pauli principle, the second is one of Kimball relations[32] and the third is due to the fact that the pair correlation function is analytic everywhere except when the distance between the two particles is zero. The smoothing of the pair correlation functions required 8 spline knots for like spins, and 5 to 6, for unlike spins.

We tabulate the pair correlation functions as a function of $r_\parallel$, for like and unlike spins, at ten different pairs of z_1 and z_2, near the edge of the positive background in tables deposited in the E-PAPS. The effects of the inhomogeneity on the pair correlation functions shown are seen in Figs. 6(a) and 6(b), where we show the contour plots of $g(z_1,z_2,r_\parallel)$ for fixed values of z_1. In Fig. 6(c) we show the contour plots for values of z_1 closer to the surface edge. The inhomogeneity effects are more pronounced in the exchange hole, since its range is larger than the range of the correlation hole. In the LDA the exchange-correlation hole is assumed to be spherically symmetric[10] and centered around the electron position. This assumption works fine in regions where the system in nearly uniform, like the center of the slab, but it breaks down in the surface where the density varies rapdly. Such effects must be taken into account for a more accurate treatment of exchange and correlation in inhomogeneous systems.

V. CONCLUSIONS

We have performed fixed-node DMC calculations for jellium slabs at five different densities, corresponding to the average valence densities of Be, Al, Mg, Li, and Na. The final DMC densities differ from the LDA densities by about 2%, confirming the initial assumption that the densities from LDA calculations are very good. The work functions computed with DMC in the calculations of a jellium slab of finite thickness were extrapolated to the semi-infinite bulk using LDA data. The reported work functions lie, on average, about 0.5 eV lower than the LDA work functions computed by Zhang *et al.*[5] This result agrees qualitatively with the work function computed in Ref. 5 using the FHNC data of Krotscheck *et al.*[8] Calculations using the Langreth-Mehl[5] GGA lie about 0.3 eV higher than LDA, while calculations using the more recent Perdew-Wang[7] GGA are lower, but not in a consistent manner. The surface energies computed with QMC are higher than the LDA energies.[5] At high densities they agree with the surface energies obtained with the Langreth-Mehl[5] GGA and at lower densities they agree with the FHNC surface energies of Krotscheck *et al.*[8] This trend is followed by the surface correlation energies. The pair correlation functions computed in this work clearly show the anisotropy of the exchange-correlation hole in regions where the density changes rapidly. We tabulated the pair correlation functions, for the range of densities computed in this work.

ACKNOWLEDGMENTS

We acknowledge useful conversations with G. Ortiz and R. M. Martin. This work has been supported by NSF Grant No. DMR-91-17822. The computational work used the Supercomputers of NCSA and the Cray-C90 of the Pittsburgh Supercomputing Center.

[1] P. Hohenberg and W. Kohn, Phys. Rev. **136**, B864 (1964).
[2] W. Kohn and L. J. Sham, Phys. Rev. **140**, A1133 (1965).
[3] P. J. Reynolds, D. M. Ceperley, B. J. Alder, and W. A. Lester, Jr., J. Chem. Phys. **77**, 5593 (1982).
[4] X.-P. Li, R. J. Needs, R. M. Martin, and D. M. Ceperley, Phys. Rev. B **45**, 6124 (1992).
[5] Z. Y. Zhang, D. C. Langreth, and J. P. Perdew, Phys. Rev. B **41**, 5674 (1990).
[6] D. C. Langreth and M. J. Mehl, Phys. Rev. B **28**, 1809 (1983); C. D. Hu and D. C. Langreth, Phys. Scr. **32**, 391 (1985).
[7] Y. Wang and J. Perdew, Phys. Rev. B **44**, 13 298 (1991); J. Perdew and Y. Wang, Phys Rev. B **45**, 13 244 (1992).
[8] E. Krotscheck, W. Kohn, and G.-X. Qian, Phys. Rev. B **32**, 5693 (1985).
[9] J. Harris and R. O. Jones, J. Phys. F **4**, 1170 (1974)
[10] O. Gunnarson and B. I. Lundqvist, Phys. Rev. B **13**, 4274 (1976).
[11] D. C. Langreth and J. P. Perdew, Phys. Rev. B **15**, 2884 (1977).
[12] See AIP Document No. E-PAPS: E-PRBMD-54-17 095-1MB for table. E-PAPS document files may be retrieved free of charge from our FTP server (http://www.aip.org/epaps/epaps.html). For further information: e-mail: paps@aip.org or fax: 516-576-2223.
[13] N. D. Lang and W. Kohn, Phys. Rev. B **1**, 4555 (1970).
[14] N. D. Lang and W. Kohn, Phys. Rev. B **3**, 1215 (1971).
[15] H. B. Shore and J. H. Rose, Phys. Rev. Lett. **66**, 2619 (1991); H. B. Shore and J. H. Rose, Phys. Rev. B **43**, 11 605 (1991).
[16] N. Metropolis, A. W. Rosembluth, M. N. Rosembluth, A. H. Teller, and E. Teller, J. Chem. Phys. **21**, 1087 (1953).
[17] D. Ceperley, Phys. Rev. B **18**, 3126 (1978).
[18] J. P. Perdew and A. Zunger, Phys. Rev. B **23**, 5048 (1981).
[19] D. M. Ceperley and B. J. Alder, Phys. Rev. Lett **45**, 566 (1980).

[20] S. Fahy, X. W. Wang, and S. G. Louie, Phys. Rev. B **42**, 3503 (1990).
[21] D. M. Ceperley and M. H. Kalos, in *Monte Carlo Methods in Statistical Physics*, edited by K. Binder (Springer-Verlag, Berlin, 1979), Chap. 4.
[22] D. M. Ceperley, Rev. Mod. Phys. **67**, 1087 (1995).
[23] D. M. Ceperley and B. J. Alder, J. Chem. Phys. **81**, 5833 (1984).
[24] Y. K. Kwon, D. M. Ceperley, and R. M. Martin, Phys. Rev. B **48**, 12 037 (1993).
[25] W. H. Press and S. A. Teukolsky, *Numerical Recipes* (Cambridge University Press, Cambridge, 1992).
[26] L. Reatto and G. L. Masserini, Phys. Rev. B **13**, 4274 (1976).
[27] S. H. Vosko, L. Wilk, and M. Nussair, Can. J. Phys. **58**, 1200 (1980).
[28] J. P. Perdew, J. A. Chevary, S. H. Vosko, K. A. Jackson, M. R. Perdeson, D. J. Singh, and C. Fiolhais, Phys. Rev. B **46**, 6671 (1992).
[29] H. J. Monkhorst and J. D. Pack, Phys. Rev. B **13**, 5188 (1976).
[30] V. Sahni and C. Q. Ma, Phys. Rev. B **22**, 5987 (1980).
[31] E. Krotscheck and W. Kohn, Phys. Rev. Lett. **57**, 862 (1986).
[32] J. D. Talman and W. F. Shadwick, Phys. Rev. A **14**, 36 (1976).
[33] T. L. Ainsworth and E. Krotscheck, Phys. Rev. B **45**, 8779 (1992).
[34] J. C. Kimball, Phys. Rev. B **14**, 2371 (1976).